

Accepted Manuscript

Normal-Inverse Bimodule Operation Hadamard Transform Ion Mobility Spectrometry

Yan Hong, Chaoqun Huang, Sheng Liu, Lei Xia, Chengyin Shen, Yannan Chu



PII: S0003-2670(18)30575-0

DOI: [10.1016/j.aca.2018.05.004](https://doi.org/10.1016/j.aca.2018.05.004)

Reference: ACA 235940

To appear in: *Analytica Chimica Acta*

Received Date: 9 February 2018

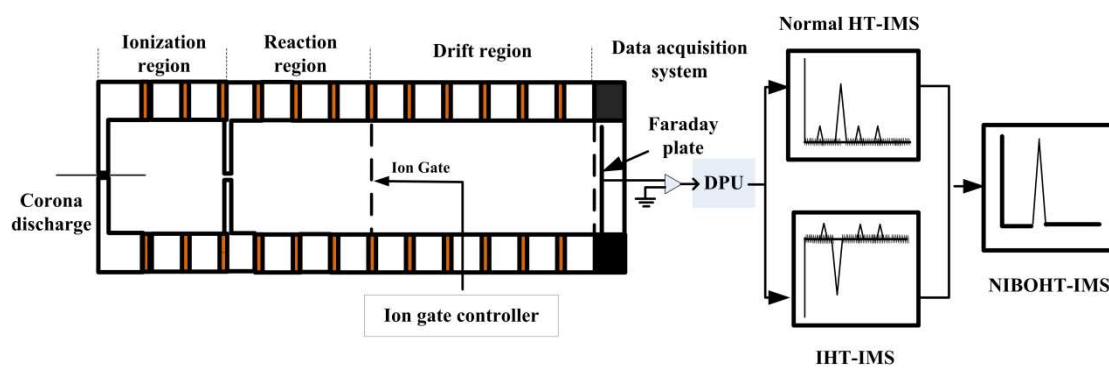
Revised Date: 25 April 2018

Accepted Date: 1 May 2018

Please cite this article as: Y. Hong, C. Huang, S. Liu, L. Xia, C. Shen, Y. Chu, Normal-Inverse Bimodule Operation Hadamard Transform Ion Mobility Spectrometry, *Analytica Chimica Acta* (2018), doi: 10.1016/j.aca.2018.05.004.

This is a PDF file of an unedited manuscript that has been accepted for publication. As a service to our customers we are providing this early version of the manuscript. The manuscript will undergo copyediting, typesetting, and review of the resulting proof before it is published in its final form. Please note that during the production process errors may be discovered which could affect the content, and all legal disclaimers that apply to the journal pertain.

Graphical Abstract



Abstract:

11 In order to suppress or eliminate the spurious peaks and improve signal-to-noise ratio (SNR)
12 of Hadamard transform ion mobility spectrometry (HT-IMS), a normal-inverse bimodule
13 operation Hadamard transform - ion mobility spectrometry (NIBOHT-IMS) technique was
14 developed. In this novel technique, a normal and inverse pseudo random binary sequence (PRBS)
15 was produced in sequential order by an ion gate controller and utilized to control the ion gate of
16 IMS, and then the normal HT-IMS mobility spectrum and the inverse HT-IMS mobility spectrum
17 were obtained. A NIBOHT-IMS mobility spectrum was gained by subtracting the inverse HT-IMS
18 mobility spectrum from normal HT-IMS mobility spectrum. Experimental results demonstrate that
19 the NIBOHT-IMS technique can significantly suppress or eliminate the spurious peaks, and
20 enhance the SNR by measuring the reactant ions. Furthermore, the gas CHCl_3 and CH_2Br_2 were
21 measured for evaluating the capability of detecting real sample. The results show that the
22 NIBOHT-IMS technique is able to eliminate the spurious peaks and improve the SNR notably not
23 only for the detection of larger ion signals but also for the detection of small ion signals.
24 **Keywords:** Ion mobility spectrometry, Hadamard transform, Signal-to-noise ratio; Spurious peaks.

25 1. Introduction

26 Ion mobility spectrometry (IMS) is an analytical technology which has been used to analyze
27 and detect trace chemical compounds, such as narcotics [1], explosives [2, 3], chemical warfare
28 agents [4-6], haloalkanes [7-9] and organic acids [10] due to its ambient pressure working
29 condition, high sensitivity, and real time monitoring capability. During a traditional IMS
30 experiment, ions which are generated in the reaction region are introduced into the drift tube under
31 the action of the ion gate pulse. Once the ion packet reaches the end of the drift tube and is
32 detected, and then the next gating event is admitted. The detected ions create ion current signal
33 and then is amplified. The output of the amplified ion signal is synchronized with the ion gate
34 pulse, yielding a mobility spectrum, i.e., a plot of ion current versus time.

35 Typically, each gate pulse is often small ($\sim 200 \mu\text{s}$) compared to that of one total period time
36 ($\sim 30\text{ms}$) in the IMS measurement. Because of this pulsing nature, IMS suffers from a low duty
37 cycle (less than 1%), which restricts the signal level as well as the sensitivity of IMS. In order to
38 overcome this problem and to increase the sensitivity of IMS, The technique of Hadamard
39 transform ion mobility spectrometry (HT-IMS) has been developed by Clowers et al. and Szumlas
40 et al. at almost the same time [11, 12]. The duty cycle of the HT-IMS was increased to 50% and
41 the signal to noise ratio (SNR) was attained to a 2-10 fold enhancement in comparison to those of
42 the traditional IMS.

43 However, some spurious peaks are always presented in the mobility spectra of HT-IMS as
44 well as the data of other multiplexing techniques [11-17]. Such unwanted peaks may lead to some
45 confusing results for the detection and also increase the baseline of spectra. Moreover, the
46 intensity of the ion signal is also reduced using the Hadamard multiplexing technique [13]. As a

47 result, the SNR suffers from a loss and is lower than the theoretical value [11].

48 The modulation defects were confirmed as the main reasons for the spurious peaks and the
49 degraded signal intensity when the Hadamard multiplexing technique is used [17]. In the case of
50 HT-IMS, imperfect ion packets of the multiplexed data and the depletion of ions in the region
51 prior to the Bradbury-Nielson gate (BNG) lead to the fluctuation of ion intensity and the existence
52 of the spurious peaks when employing a BNG. The effect of modulation defects due to imperfect
53 gating was minimized by discarding part of the multiplexed ion signal [11]. Moreover, a flexible
54 “digital multiplexing” method has been developed by Kwasnik et al. The duty cycle was variable
55 from 0.5% to 50% and the SNR was increased to 2~7 folds using this technique. The spurious
56 peaks were also reduced or eliminated [14]. Prost et al. have developed an algorithm to identify
57 and remove the data artifacts, i.e. spurious peaks. Following application of this method, the
58 spurious peaks were avoided and the sensitivity was increased in the experiment of ion mobility
59 spectrometry-mass spectrometry (IMS-MS) [13]. Additionally, Puton et al. have reported that the
60 shapes of ion swarms on the beginning of drift region may lead to the peak deformation and
61 generates the spurious peaks. The fluctuations of the baseline also make the contribution to those
62 spurious peaks [18, 19]. Our group also focuses on the study of Hadamard multiplexing technique
63 [15, 16, 20, 21] and has developed an inverse Hadamard transform ion mobility spectrometry
64 (IHT-IMS) technique. With this IHT-IMS technique, the spurious peaks were identified rapidly
65 [15].

66 In this study, a normal-inverse bimodule operation Hadamard transform - ion mobility
67 spectrometry (NIBOHT-IMS) technique is reported. In this method, a normal and an inverse
68 pseudo random binary sequence (PRBS) was produced in sequential order by an ion gate

69 controller and utilized to control the ion gate of IMS, respectively, and then the normal HT-IMS
70 mobility spectrum and the inverse HT-IMS mobility spectrum were obtained. A NIBOHT-IMS
71 mobility spectrum was gained by subtracting the inverse HT-IMS mobility spectrum from normal
72 HT-IMS mobility spectrum. With the application of the NIBOHT-IMS technique, the spurious
73 peaks are reduced or almost eliminated. Furthermore, the ion signal intensity and the SNR are
74 enhanced notably.

75 **2. Experimental section**

76 The homemade atmospheric pressure corona discharge ion mobility spectrometry (APCD-
77 -IMS) with the function of NIBOHT-IMS is demonstrated schematically in Fig. 1. The detailed
78 description about the APCD-IMS was shown in our previous work [22]. Briefly, it consists of the
79 ionization region, the reaction region, the Bradbury-Nielson ion gate, and the drift region and data
80 acquisition unit.

81 In the ionization region, the discharge electrodes with the geometry of point to plate were
82 installed coaxially and located at the top of the IMS tube. The reactant ions were generated in this
83 region by means of negative corona discharge through dried air and dragged into the reaction
84 region. Both the reaction and drift regions consist of metal guards which were insulated from each
85 other using Teflon rings. The high voltage through an electric resistance network on the metal
86 rings generated a weak homogeneous electric field along the central axis of the drift tube. At the
87 interface between the reaction and drift region, a BNG ion gate is installed and works under the
88 control of an ion gate controller. When the ion gate is opened for a short time, the product ions and
89 the reactant ions swarm into the drift region and drift toward a Faraday plate under the function of
90 the applied homogeneous electric field. And then, the current signal will be generated by

91 collecting the ions with a Faraday plate and amplified by a current amplifier (Keithley 428). After
92 that, it is fed into the computer data processing unit (DPU). The IMS works under the negative
93 detection mode and all the experiments are performed under the condition of 295 K and ambient
94 pressure. The relative humidity in the lab is about 43%.

95 **3. The principle of the IIMS, the HT-IMS, the IHT-IMS and the** 96 **NIBOHT-IMS**

97 **IIMS**

98 Tabrizchi and Jazan have introduced Inverse IMS (IIMS) in 2010 [23]. In this method, an
99 inverse pulse was applied to the ion gate, which means the ion gate is opened for a long duration
100 and closed for a short period. Thus, the gate of the IIMS introduces "a dip" into a continuous ion
101 beam instead of ion bundles, so that a 1% duty cycle electronic pulse in inverse mode admits
102 ~99% of the available ion stream. In this case, the ions are distributed outside of the dip and
103 repulse each other. This repulsion effect of charged ions leads to the compression of the dip,
104 namely the improvement of resolving power [24]. The resolving power of the IIMS was enhanced
105 about 30%-60% compared with the conventional IMS.

106 **HT-IMS**

107 In HT-IMS technique, a pseudo random binary sequence (PRBS) is used as the modulation
108 sequence to perform the Hadamard multiplexing [11, 12]. Considering a PRBS, such as
109 "101001011110...", symbol "0" means the low level output which is used to shut the ion injection
110 for a period, whereas the symbol "1" represents the high level output which is utilized to activate
111 the ion injection. As a result, the convoluted data, namely the superposition of a series of ion
112 mobility spectra are obtained under the control of a pseudo-random binary gating function. The

113 convolution of the conventional Hadamard multiplexing is demonstrated in Eq. 1.

$$114 \quad [\mathbf{Y}] = [\mathbf{S}] \times [\mathbf{X}] \quad (1)$$

115 Where Y corresponds to the convolution spectrum which is encoded by multiple normal spectra, S
 116 is the $n \times n$ (n is the length of PRBS) matrix which is generated by PRBS, and X corresponds to
 117 a series of single spectrum which is derived from a single injection. To reconstruct the original
 118 signal X, the superimposed signal is deconvoluted by multiplication of the inverse S-matrix S^{-1} as
 119 shown in Eq. 2.

$$120 \quad [\mathbf{X}]^* = [\mathbf{S}]^{-1} \times [\mathbf{Y}] = [\mathbf{S}]^{-1} \times [\mathbf{S}] \times [\mathbf{X}] \quad (2)$$

121 **IHT-IMS**

122 Recently, an inverse Hadamard transform ion mobility spectrometry (IHT-IMS) was
 123 developed [15, 16]. The principle of this technique is briefly described as below. Under the IHT
 124 mode, the modulation PRBS was inverted by the ion gate controller. Thus, if the normal PRBS is
 125 “101001011110...”, the gating pulse for IHT-IMS will be “010110100001...”. Here the symbol
 126 “0” means the low level output which is still used to shut the ion gate, whereas the symbol “1”
 127 represents the high level output which is used to open the ion gate. According to the principle of
 128 the IIMS, the convoluted data consists of the superposition of multiple "dips" rather than "peaks".
 129 Under this inverse Hadamard transform control mode, the inverse HT-IMS mobility spectrum was
 130 attained. Also the spurious peaks still exist in the results of IHT-IMS [16].

131 **NIBOHT-IMS**

132 With the combination of the HT-IMS and the IHT-IMS, a normal-inverse bimodule operation
 133 Hadamard transform - ion mobility spectrometry (NIBOHT-IMS) technique is proposed in this
 134 report. In this NIBOHT-IMS technique, the ion gate controller can generate a normal and an
 135 inverse PRBS in sequential order, which is used to control the BNG ion gate as shown in Fig. 1.

136 The PRBS also contains a pseudo random sequence which includes a series of “1” and “0”, such
137 as “0010001111...”. In the case of the normal HT-IMS control mode, a normal PRBS is generated.
138 The convoluted ion signals which are composed of a series of ion mobility spectra are obtained
139 under the control of this normal pseudo-random gating function and then they will be
140 deconvoluted to a normal HT-IMS mobility spectrum. After that, the ion gate controller generates
141 an inverse PRBS; an inverse HT-IMS mobility spectrum is attained. Because of the nature of
142 PRBS and inverse PRBS, the phase of real signal will be changed to the opposite, whereas the
143 phase of the spurious peaks will be the same [15]. Finally, the NIBOHT-IMS mobility spectrum is
144 attained by subtracting the inverse HT-IMS mobility spectrum from the normal HT-IMS mobility
145 spectrum. Most of those spurious peaks will be suppressed or even removed and the SNR will be
146 increased accordingly.

147 **4. Results and discussion**

148 **4.1 The measurements of the reactant ions using the conventional IMS, the normal HT-IMS,** 149 **the IHT-IMS and the NIBOHT-IMS technique**

150 In this section, only reactant ions produced via negative corona discharge in air were
151 considered. The uniform electric field in the drift region was set as 300 Vcm^{-1} . The ion gate pulse
152 width for all the experiments was $200 \mu\text{s}$. The order of the S-matrix is 255 in this report except
153 those specified experiments.

154 As shown in Fig. 2, the spectra of reactant ions measured using the conventional IMS, the
155 normal HT-IMS, the IHT-IMS and the NIBOHT-IMS are illustrated. The total scan time for
156 Hadamard multiplexing is about 51 ms when the order of the S-matrix is 255 and the gating pulse
157 width is $200 \mu\text{s}$. In order to get the better comparison, the ion signal of conventional IMS was

158 averaged two times to keep its acquisition time is almost the same as that of Hadamard
159 multiplexing methods. Fig. 2(a) shows that the maximum ion intensity is about -1915 and the
160 baseline has a distinct fluctuation in the data of the conventional IMS. The SNR of the
161 conventional IMS mobility spectra were calculated to be 12.7 using the equation $SNR = \frac{H}{\sigma}$
162 respectively, where H is the height of the reactant ion peak (RIP), corresponding to the component
163 concerned, and measured from the maximum of the peak to the extrapolated baseline of the signal
164 and σ is the standard deviation of the baseline in the spectrum [25]. Moreover, the maximum ion
165 intensity is decreased to -713, whereas the SNR is increased to 28.2, which is lower than the
166 theoretical value under the normal HT-IMS mode. Some spurious peaks with the same phase of
167 the real signal are presented as shown in Fig. 2(b). Using the IHT-IMS method, the maximum ion
168 intensity is also decreased, which leads to the reduction of the SNR. However, the real signal peak
169 changes to the positive direction, whereas those spurious peaks still show the negative direction as
170 in our previous investigation [15]. The positions of the spurious peaks in the normal HT-IMS and
171 IHT-IMS are almost the same due to the nature of PRBS and inverse PRBS as discussed above.
172 Fig. 2 (d) shows the result measured by the NIBOHT-IMS technique. With this control mode, the
173 spurious peaks are almost eliminated and the maximum ion intensity of RIP is increased two folds
174 in comparison to that of the normal HT-IMS and inverse HT-IMS. The SNR is increased to 43.6,
175 which is about 3.6 folds of that of the conventional IMS.

176 **4.2 The effect of the order of S-matrix**

177 In order to investigate the effect of the different order of S-matrix using the NIBOHT-IMS
178 method, the reactant ions were measured using the conventional IMS, the normal HT-IMS, the
179 IHT-IMS and the NIBOHT-IMS with different orders of S - matrix. The results are demonstrated

180 in Fig. 3 and Fig. 4.

181 Fig. 3 shows the results measured using the conventional IMS, the normal HT-IMS, the
182 IHT-IMS and the NIBOHT-IMS when the order of S - matrix is 511 in the Hadamard multiplexing
183 method. As shown in Fig. 3(a), the maximum ion intensity and the SNR are -1808 and 12.1
184 respectively in the conventional IMS. However, the maximum ion intensity is decreased to -940,
185 whereas the SNR is increased to 32.1 under the normal HT-IMS mode as shown in Fig. 3(b). Fig.
186 3(c) shows the maximum ion intensity is also decreased using the IHT-IMS method. And the SNR
187 is still lower than the theoretical value. Besides that, the real signal peak changes to the positive
188 direction, whereas those spurious peaks still keep the negative direction. However, the maximum
189 ion intensity and the SNR are almost 2 folds of those of normal/inverse HT-IMS with the
190 application of the NIBOHT-IMS. Additionally, the spurious peaks are suppressed under the
191 NIBOHT-IMS mode as shown in the Fig. 3(d).

192 Similarly, the reactant ions were also measured using the conventional IMS, the normal
193 HT-IMS, the IHT-IMS and the NIBOHT-IMS, where the S-matrix order used in the HT method is
194 changed to 1023. As shown in Fig. 4, the maximum ion intensity in NIBOHT-IMS is also two
195 times as high as that of the normal/inverse HT-IMS. A 2.9 - fold and 3.2 -fold increases in the
196 SNR for the normal and inverse HT-IMS are attained respectively in comparison to that of the
197 conventional IMS, whereas the enhancement of the SNR in the NIBOHT-IMS is about 8 folds.
198 Moreover, some distinct spurious peaks are removed in the data of the NIBOHT-IMS.

199 Combining Fig.2, Fig.3 and Fig.4, we found that the increased tendency of the SNR is a
200 function of sequence length in Hadamard multiplexing method. The SNR increased with the
201 increase of the length of S-matrix order. The same phenomenon has been also observed by

202 Clowers et al [11]. Additionally, it is noted that the spurious peaks in the NIBOHT-IMS haven't
203 been eliminated completely as shown in Fig. 3(d) and Fig. 4(d). Ideally, the position and the
204 intensities of spurious peaks should be almost the same under the normal HT-IMS and IHT-IMS
205 control mode as mentioned above, which means that those spurious peaks will be removed
206 completely with the application of NIBOHT-IMS. However, the repulsion effect among the
207 charged ions in drift region plays a different role under the normal HT-IMS and IHT-IMS control
208 mode [16], which would lead to a little shift at the position of the spurious peaks or generating
209 some uncertain spurious peaks. Therefore a few spurious peaks with low intensity still exist in the
210 results of NIBOHT-IMS. Anyway, the ion intensity and the SNR still have a notable enhancement
211 using the NIBOHT-IMS.

212 Furthermore, the acquisition time will be extended using the NIBOHT-IMS method. If the
213 order of the S-matrix is 255, the gating pulse width is 200 μ s, the total scan time for conventional
214 Hadamard multiplexing will be about 51 ms, and the time consumption for the data acquisition
215 (sampling, A/D conversion, decoding, and data presentation) will be about 1.5 s. As a result, the
216 data acquisition time will be doubled (\sim 3 s) under the NIBOHT-IMS measurement. When the
217 length of S-matrix order is increased to 1023, the data acquisition time will be only about 12 s.
218 The time cost is still acceptable for the fast detection of the IMS.

219 **4.3 Sample detection using the NIBOHT-IMS**

220 **Measurement of CHCl_3 .**

221 To further evaluate the capability of the NIBOHT-IMS technique, the gas sample CHCl_3 was
222 measured by a home-made atmospheric pressure nitrogen corona discharge ion mobility
223 spectrometry apparatus (APNCD-IMS) which can be referred to in our previous report [7-9].
224 Different from the APCD-IMS apparatus, an additional curtain region located between the

225 ionization region and the reaction region is used to prevent the sample gases from diffusing into
226 the ionization region. In the ionization region, thermal electrons were generated by means of
227 negative corona discharge through nitrogen gas at atmospheric pressure. The gas samples were
228 introduced into the reaction region by carrier gas N_2 and attached by the thermal low-energy
229 electrons which were dragged from the ionization region. The product ions were formed by the
230 interaction between the low-energy electrons and the gas sample. The uniform electric field in the
231 drift region is 480 Vcm^{-1} . The order of the S-matrix is 255.

232 Gas sample CHCl_3 . (~480ppb) was injected into the IMS cell by syringe pump and measured
233 using the conventional IMS, the normal HT-IMS, the IHT-IMS and the NIBOHT-IMS respectively.
234 As shown in Fig. 5, two product ions (labeled with "1" and "2") were observed. The intensities of
235 the product ion peaks in the results of the NIBOHT-IMS are nearly twice as those of the normal
236 HT and the inverse HT method. The SNR was calculated to be 23.6, 108.5 and 105.7 respectively
237 in the conventional IMS, the normal HT-IMS and the IHT-IMS using the peak "1". With the
238 application of the NIBOHT-IMS, the spurious peaks are almost eliminated and the SNR is 8.9-fold
239 and 1.9-fold enhancement respectively in comparison to that of the conventional IMS and the
240 normal/inverse HT-IMS respectively as shown in Fig. 5(d). The enhancement of the SNR will be
241 increased much higher with the increasing of the order of S-matrix as discussed above.

242 **Measurement of CH_2Br_2**

243 The SNR is enhanced and the spurious peaks are almost removed for the detection of lager
244 ion signal as discussed above. In this section gas sample CH_2Br_2 was measured for evaluating the
245 detection capability of the small ion signal using the NIBOHT-IMS technique. There are two
246 products for the low energy electron attachment of CH_2Br_2 as our previous investigation [26].

247 During the experiments, about 5 ppm CH_2Br_2 was injected into the IMS cell for the measurements
248 by the conventional IMS, the normal HT-IMS, the IHT-IMS and the NIBOHT-IMS. As shown in
249 the Fig. 6(a), one distinct larger peak labeled with "1" was observed at 9.05 ms. However the peak
250 "2" is almost confused with the baseline noise and is very hard to be distinguished. The SNR was
251 calculated to be only 4.8 using the peak "2". Under the HT-IMS and IHT-IMS mode, the peak "2"
252 can be clearly distinguished. The SNR was increased to 13.4 and 12.9 respectively. Unfortunately,
253 some distinct spurious peaks were observed as shown in Fig. 6(b) and (c). Fig. 6(d) shows the
254 results of the NIBOHT-IMS. The spurious peaks are suppressed remarkably in comparison to
255 those of the results of the HT-IMS and IHT-IMS. The peak "2" can be clearly resolved and the
256 SNR was calculated to be 26.9, which is about 5-fold and 2-fold enhancement respectively in
257 comparison to that of conventional IMS and the normal/inverse HT-IMS. The results validate that
258 the NIBOHT-IMS technique is still effective for the detection of the weak ion signals.

259 5. Conclusion

260 In this report, in order to suppress or eliminate the spurious peaks and increase the SNR in
261 the data of Hadamard multiplexing technique, a normal-inverse bimodule operation Hadamard
262 transform - ion mobility spectrometry (NIBOHT-IMS) technique was developed. The ion intensity
263 and the SNR in the NIBOHT-IMS were enhanced over the normal and inverse HT-IMS by
264 measuring the reactant ion. The spurious peaks were suppressed or removed effectively.
265 Furthermore, the gas sample CHCl_3 and CH_2Br_2 was measured for evaluating its ability to detect
266 larger and small ion signals using the NIBOHT-IMS technique. The spurious peaks are almost
267 removed and the SNR was enhanced remarkably with the application of the NIBOHT-IMS.

268 **ACKNOWLEDGMENTS**

269 This work was supported by National Natural Science Foundation of China (No. 61671434,
270 21477132), Provincial Natural Foundation of Anhui Province (No.1808085MF169), Natural
271 Science Research Project of Anhui Universities (No. KJ2018A0086) and Provincial Science and
272 Technology Major Project of Anhui Province (No.17030801035)

273 **References**

- 274 [1] C. Fuche, J. Deseille, Ion mobility spectrometry: a tool to detect narcotics and explosives, *Actual.*
275 *Chim.* (2010) 91-95.
- 276 [2] R.G. Ewing, D.A. Atkinson, G.A. Eiceman, G.J. Ewing, A critical review of ion mobility
277 spectrometry for the detection of explosives and explosive related compounds, *Talanta* 54 (2001)
278 515-529.
- 279 [3] K.M. Roscioli, E. Davis, W.F. Siems, A. Mariano, W.S. Su, S.K. Guharay, H.H. Hill, Modular Ion
280 Mobility Spectrometer for Explosives Detection Using Corona Ionization, *Anal. Chem.* 83 (2011)
281 5965-5971.
- 282 [4] W.E. Steiner, B.H. Clowers, L.M. Matz, W.F. Siems, H.H. Hill, Rapid screening of aqueous
283 chemical warfare agent degradation products: Ambient pressure ion mobility mass spectrometry,
284 *Anal. Chem.* 74 (2002) 4343-4352.
- 285 [5] S. Zimmermann, S. Barth, W.K.M. Baether, J. Ringer, Miniaturized low-cost ion mobility
286 spectrometer for fast detection of chemical warfare agents, *Anal. Chem.* 80 (2008) 6671-6676.
- 287 [6] M.A. Makinen, O.A. Anttalainen, M.E.T. Sillanpaa, Ion mobility spectrometry and its applications
288 in detection of chemical warfare agents, *Anal. Chem.* 82 (2010) 9594-9600.
- 289 [7] H.T. Feng, W.Q. Niu, H.Y. Han, C.Q. Huang, H.M. Wang, J. Matuska, M. Sabo, S. Matejcik, H.H.
290 Jiang, Y.N. Chu, Rate constants of electron attachment to chlorobenzenes measured by atmospheric
291 pressure nitrogen corona discharge electron attachment ion mobility spectrometry, *Int. J. Mass*
292 *Spectrom.* 305 (2011) 30-34.
- 293 [8] H. Gao, W.Q. Niu, C.Q. Huang, Y. Hong, C.Y. Shen, H.M. Wang, Y. Lu, X.J. Chen, L. Xia, H.H.
294 Jiang, Y.N. Chu, Rate constants of electron attachment to alkyl iodides measured by photoionization
295 electron attachment ion mobility spectrometry (PI-EA-IMS), *Int. J. Mass Spectrom.* 376 (2015) 1-5.
- 296 [9] C.Q. Huang, B.B. Xu, W.Q. Niu, H. Gao, Y. Hong, L. Xia, Y. Lu, C.Y. Shen, Y.N. Chu, An
297 experimental study of low energy electrons attachment to CH₂ClBr using ion mobility
298 spectrometry, *Int. J. Mass Spectrom.* 402 (2016) 29-35.
- 299 [10] H. Gao, W.Q. Niu, Y. Hong, B.B. Xu, C.Y. Shen, C.Q. Huang, H.H. Jiang, Y.N. Chu, Negative
300 photoionization chloride ion attachment ion mobility spectrometry for the detection of organic
301 acids, *RSC Adv.* 4 (2014) 63977-63984.
- 302 [11] B.H. Clowers, W.F. Siems, H.H. Hill, S.M. Massick, Hadamard transform ion mobility
303 spectrometry, *Anal. Chem.* 78 (2006) 44-51.
- 304 [12] A.W. Szumlas, S.J. Ray, G.M. Hieftje, Hadamard transform ion mobility spectrometry, *Anal.*
305 *Chem.* 78 (2006) 4474-4481.

- 306 [13] S.A. Prost, K.L. Crowell, E.S. Baker, Y.M. Ibrahim, B.H. Clowers, M.E. Monroe, G.A. Anderson,
307 R.D. Smith, S.H. Payne, Detecting and removing data artifacts in Hadamard transform ion
308 mobility-mass spectrometry measurements, *J. Am. Soc. Mass Spectrom.* 25 (2014) 2020-2027.
- 309 [14] M. Kwasnik, J. Caramore, F.M. Fernandez, Digitally-multiplexed nanoelectrospray ionization
310 atmospheric pressure drift tube ion mobility spectrometry, *Anal. Chem.* 81 (2009) 1587-1594.
- 311 [15] Y. Hong, W.Q. Niu, H. Gao, L. Xia, C.Q. Huang, C.Y. Shen, H.H. Jiang, Y.N. Chu, Rapid
312 identification of false peaks in the spectrum of Hadamard transform ion mobility spectrometry with
313 inverse gating technique, *RSC Adv.* 5 (2015) 56103-56109.
- 314 [16] Y. Hong, S. Liu, C.Q. Huang, L. Xia, C.Y. Shen, H.H. Jiang, Y.N. Chu, Simultaneous
315 improvement of resolving power and signal-to-noise ratio using a modified Hadamard
316 transform-inverse ion mobility spectrometry technique, *J. Am. Soc. Mass Spectrom.* 28 (2017)
317 2500-2507.
- 318 [17] J.R. Kimmel, F.M. Fernandez, R.N. Zare, Effects of modulation defects on Hadamard transform
319 time-of-flight mass spectrometry (HT-TOFMS), *J. Am. Soc. Mass Spectrom.* 14 (2003) 278-286.
- 320 [18] J. Puton, A. Knap, B. Siodlowski, Modelling of penetration of ions through a shutter grid in ion
321 mobility spectrometers, *Sensors Actuat B-Chem.* 135 (2008) 116-121.
- 322 [19] F.K. Tadjimukhamedov, J. Puton, J.A. Stone, G.A. Eiceman, A study of the performance of an ion
323 shutter for drift tubes in atmospheric pressure ion mobility spectrometry: Computer models and
324 experimental findings, *Rev. Sci. Instrum.* 80 (2009).
- 325 [20] Y. Fang, W. Niu, C. Shen, S. Liu, C. Huang, H. Wang, H. Jiang, Y. Chu, A preliminary theoretical
326 simulation of Hadamard transform of ion mobility spectrometry, *Chinese J. Quantum Electronics* 30
327 (2013) 524-529.
- 328 [21] Y. Hong, C. Huang, C. Shen, Y. Chu, Effects of multiplexing parameters on Hadamard transform
329 ion mobility spectrometry, *Chinese J. Quantum Electronics* 34 (2017) 140-144.
- 330 [22] S. Liu, C.Q. Huang, C.Y. Shen, H.H. Jiang, Y.N. Chu, A novel driving mode for ion shutter based
331 on alternating current superposition and its application to ion mobility spectrometry, *Sens. Actuator*
332 *B-Chem.* 211 (2015) 102-110.
- 333 [23] M. Tabrizchi, E. Jazan, Inverse ion mobility spectrometry, *Anal. Chem.* 82 (2010) 746-750.
- 334 [24] V. Ilbeigi, M. Tabrizchi, Peak-peak repulsion in ion mobility spectrometry, *Anal. Chem.* 84 (2012)
335 3669-3675.
- 336 [25] R. Cumeras, E. Figueras, C.E. Davis, J.I. Baumbach, I. Gracia, Review on Ion Mobility
337 Spectrometry. Part 2: hyphenated methods and effects of experimental parameters, *Analyst* 140
338 (2015) 1391-1410.
- 339 [26] B.B. Xu, W.Q. Niu, H. Gao, Y. Hong, C.Y. Shen, H.M. Wang, C.Q. Huang, H.H. Jiang, Y.N. Chu,
340 Rate constants of electron attachment to brominated methanes measured by corona discharge ion
341 mobility spectrometry, *Chinese J. Quantum Electronics* 1 (2016) 88-92.
- 342
- 343

344

Figure Captions

345 Fig. 1 Schematic diagram of the normal-inverse bimodule operation Hadamard transform - ion
346 mobility spectrometry. The ion signal in this figure is a negative detection mode.

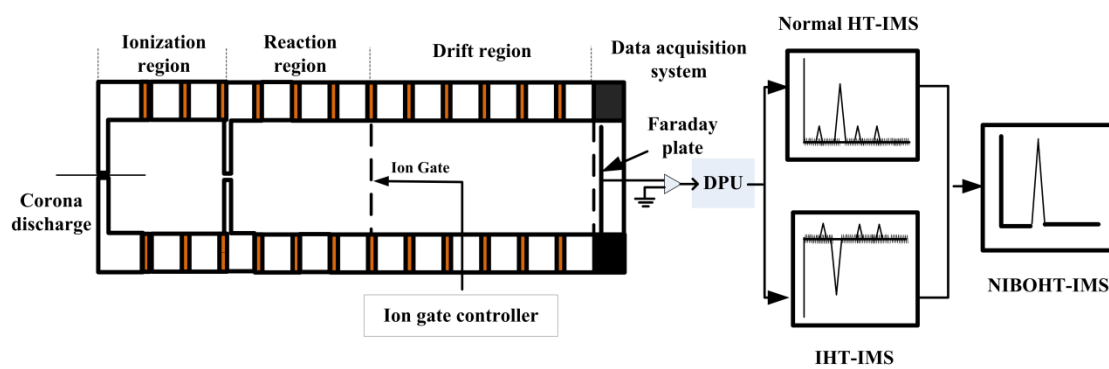
347 Fig.2 The ion mobility spectra of the reaction ions measured by (a) the conventional IMS (b) the
348 normal HT-IMS. (c) the IHT-IMS and (d) the NIBOHT-IMS. Here the order of the S-matrix is 255
349 in the Hadamard multiplexing data.

350 Fig. 3 The ion mobility spectra of the reaction ions measured by (a) the conventional IMS (b) the
351 normal HT-IMS (c) the IHT-IMS and (d) the NIBOHT-IMS. Here the order of the S-matrix is 511
352 in the Hadamard multiplexing data.

353 Fig.4 The ion mobility spectra of the reaction ions measured by (a) the conventional IMS (b) the
354 normal HT-IMS (c) the IHT-IMS and (d) the NIBOHT-IMS. Here the order of the S-matrix is
355 1023 in the Hadamard multiplexing data.

356 Fig. 5 The ion mobility spectra of CHCl_3 measured by (a) the conventional IMS (b) the normal
357 HT-IMS (c) the IHT-IMS and (d) the NIBOHT-IMS. Here the order of the S-matrix is 255 in the
358 Hadamard multiplexing data and the SNR was calculated by peak "1".

359 Fig. 6 The ion mobility spectra of CH_2Br_2 measured by (a) the conventional IMS (b) the normal
360 HT-IMS (c) the IHT-IMS and (d) the NIBOHT-IMS. Here the order of the S-matrix is 255 in the
361 Hadamard multiplexing data and the SNR was calculated by peak "2"

362 **Fig.1**

363

364 **Fig.2**

365

366

367 **Fig.3**
368



369
370

371 **Fig. 4**
372



373
374

375 **Fig. 5**
376



377
378
379

380

381 **Fig. 6**

382



383

384

Figure Captions

Fig. 1 Schematic diagram of the normal-inverse bimodule operation Hadamard transform - ion mobility spectrometry. The ion signal in this figure is a negative detection mode.

Fig.2 The ion mobility spectra of the reaction ions measured by (a) the conventional IMS (b) the normal HT-IMS. (c) the IHT-IMS and (d) the NIBOHT-IMS. Here the order of the S-matrix is 255 in the Hadamard multiplexing data.

Fig. 3 The ion mobility spectra of the reaction ions measured by (a) the conventional IMS (b) the normal HT-IMS (c) the IHT-IMS and (d) the NIBOHT-IMS. Here the order of the S-matrix is 511 in the Hadamard multiplexing data.

Fig.4 The ion mobility spectra of the reaction ions measured by (a) the conventional IMS (b) the normal HT-IMS (c) the IHT-IMS and (d) the NIBOHT-IMS. Here the order of the S-matrix is 1023 in the Hadamard multiplexing data.

Fig. 5 The ion mobility spectra of CHCl_3 measured by (a) the conventional IMS (b) the normal HT-IMS (c) the IHT-IMS and (d) the NIBOHT-IMS. Here the order of the S-matrix is 255 in the Hadamard multiplexing data and the SNR was calculated by peak "1".

Fig. 6 The ion mobility spectra of CH_2Br_2 measured by (a) the conventional IMS (b) the normal HT-IMS (c) the IHT-IMS and (d) the NIBOHT-IMS. Here the order of the S-matrix is 255 in the Hadamard multiplexing data and the SNR was calculated by peak "2"

Fig.1

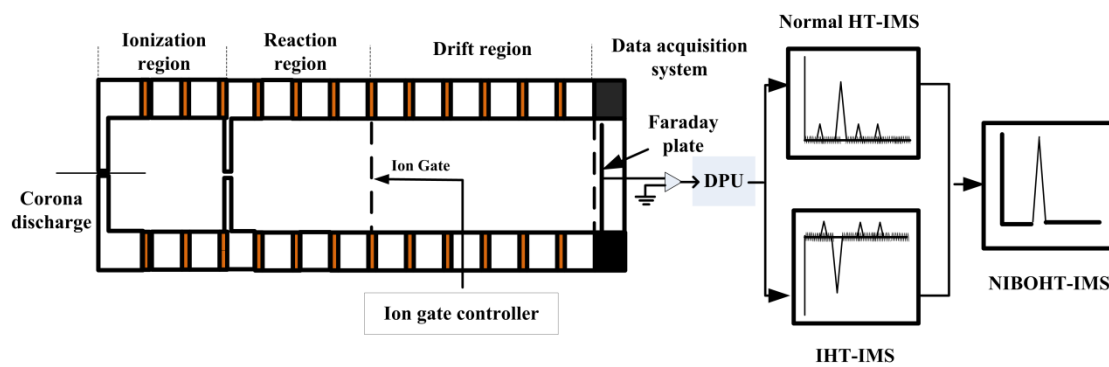


Fig.2

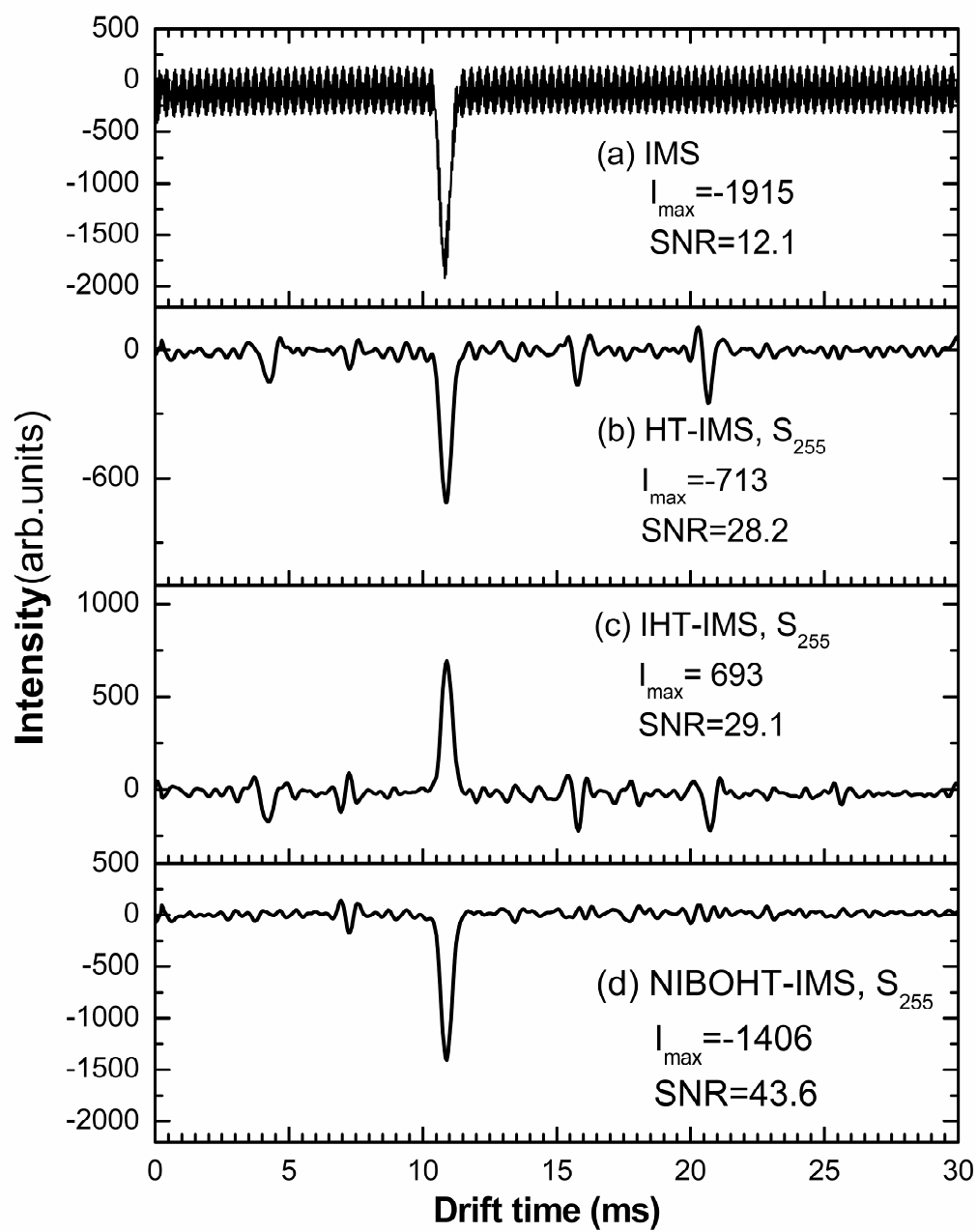


Fig.3

Fig. 4

Fig. 5

Fig. 6



Highlights

1. A normal-inverse bimodule operation Hadamard transform - ion mobility spectrometry (NIBOHT-IMS) technique was developed for the first time.
2. Experimental results demonstrate that the NIBOHT-IMS technique can significantly suppress or eliminate the spurious peaks
3. The SNR was enhanced with the application of the NIBOHT-IMS not only for the detection of larger ion signals but also for the detection of small ion signals.